Available online at www.sciencedirect.com
ScienceDirect
Journal of Computational Physics 223 (2007) 416–435
JOURNAL OF COMPUTATIONAL PHYSICS
www.elsevier.com/locate/jcp

A boundary element formulation of protein electrostatics with explicit ions

Weidong Xin, André H. Juffer *

The Biocenter and the Department of Biochemistry, University of Oulu, P.O. Box 3000, FIN-90014, University of Oulu, Finland

Received 28 November 2005; received in revised form 8 August 2006; accepted 19 September 2006
Available online 1 November 2006

Abstract

A novel formulation based upon continuum electrostatics to compute the electrostatic potential in and around two biomolecules in a solvent with ionic strength is presented. Many, if not all, current methods rely on the non-linear Poisson–Boltzmann equation to include ionic strength. The present formulation, however, describes ionic strength through the inclusion of explicit ions, which considerably extends its applicability and validity range. The method relies on the boundary element method and results in two very similar coupled integral equations valid on the dielectric boundaries of two molecules, respectively. The method can be employed to estimate the total electrostatic energy of two protein molecules at a given distance and orientation in an electrolyte solution with zero to moderately high ionic strength. The formulation is equally applicable to the case of a single solute in an electrolyte. A number of Monte Carlo simulations of protein-like solutes in NaCl at various concentrations have been performed and demonstrates the method's usefulness to estimate the electrostatic contribution to the potential of mean force between two biomolecules in an electrolyte.

Keywords: Protein; Electrostatics; Boundary element method; Ionic strength; Explicit ions; Potential of mean force; Computer simulation; Coarse-grained model

1. Introduction

Electrostatic interactions play a dominant role in most, if not all, biological processes involving proteins and other biomolecules. Because of their long ranged character, special care must be taken to ensure an accurate calculation [1]. Methods based upon continuum electrostatics (that is, without atomic detail) are very popular [2,3] and have found widespread application. They have been employed for, among other things, the calculation of protein ligand affinities [4,5], the prediction of acid dissociation constants [6,7], an investigation of the effects of point mutations in proteins [8], the computation of solvation free energies of small molecules [9], and the prediction of protein stability [10]. Continuum electrostatics was also combined with quantum chemistry approaches to account for solvent effects [11,12]. One reason for the popularity and

* Corresponding author. Tel.: +358 8 553 1161; fax: +358 8 553 1141.
E-mail address: andre.juffer@oulu.fi (A.H. Juffer).

0021-9991/$ - see front matter
doi:10.1016/j.jcp.2006.09.011

success of continuum electrostatics is that these methods include the important effect of polarization due to differences in the dielectric properties of the protein and the surrounding solvent [13]. This type of polarization is still commonly ignored in, for instance, classical force fields for biomolecular simulation.

There exists a wide variety of calculation methods that rely upon continuum electrostatics. Among these, the most popular relies on the Poisson–Boltzmann (PB) equation and the finite difference method. This method maps a given protein/solvent system onto a three dimensional grid and the PB equation is solved at the grid points. Subsequently, the total electrostatic energy of the system is obtained [1,14,15]. The boundary element method (BEM), the main topic of this work, offers an attractive alternative because of its higher intrinsic accuracy. The method starts from the same set of differential equations to describe a protein/solvent system, but converts this into a set of integral equations valid on a surface or a dielectric boundary enclosing the protein of interest [16,17]. Discretization of these integral equations results in a matrix equation, the solution of which, under conditions of non-zero ionic strength, corresponds to the total electrostatic potential and the normal component of the total electrostatic field on the boundary [17,18]. Subsequently, the total electrostatic potential and the total electrostatic field can be computed in the protein or solvent region by a simple numerical integration across the boundary. The electrostatic energy is then easily obtained from the total potential and, consequently, the electrostatic forces are readily available [19]. The BEM cleanly separates in a natural way the reaction potential from the direct Coulombic terms, the latter being calculated in an exact manner, so that any numerical error in the total potential and field solely arises from the computation of the reaction potential and field. It should be noted that Zhou et al. [20] have introduced a finite difference formulation that also completely eliminates the need to compute the self-energy term. In addition, recent developments such as adaptive finite element methods [21–23] and focused finite differencing [24] have greatly improved the accuracy of traditional finite difference and finite element methods as well.

In recent years, the BEM has been used, among other things, to compute solvation free energies of small molecules [9], to study protein folding [25], to predict acid-dissociation constants in proteins [7], to compute the affinity of a protein for a charged surface carrying an uniform charge density [26], to estimate the interaction energy and forces between two or more proteins [27–30,33], to calculate the affinities of peptides for proteins [5], to consider the electrostatic recognition between enzyme and inhibitor [31], to describe solvent effects in quantum chemistry approaches [11], and to include electrostatic interactions in the framework of the generalized Langevin equation [32,33].

In this work, the main objective is to introduce a novel formulation of the boundary element method. We present here a formulation that describes ionic strength by means of *explicit ions*. The usage of explicit ions in the description of biomolecular systems is not a new idea, but the effects of dielectric boundaries in such formulations have simply been ignored or were deemed irrelevant [34]. All existing BEM implementations are based upon a full continuum description of the solvent to accommodate ionic strength and rely on the linear PB equation [17,27,28]. The linear PB equation is valid only at very low ionic strengths. It may be possible to extend existing BEM formulations by means of the non-linear PB equation, as was already implemented for the finite difference method [35], but this seems not feasible with a BEM approach, although a 'hybrid' method has been proposed [36,37]. It is rather questionable to rely on the non-linear PB equation given the fact that only the linear PB is an exact limiting law of statistical mechanical theories of electrolyte solutions [38]. Any continuum approach to simulate electrolyte solutions ignores ion–ion correlation, which is already significant at concentrations as low as 0.01 M [39]. Also, the concept of electroneutrality is not very well defined in pure continuum approaches, while special measures to account for the ion-exclusion layer may be required as well [37]. The method presented in this work overcomes these limitations through the use of explicit ions and, combined with a Monte Carlo simulation approach (or any other appropriate simulation method, e.g. Brownian dynamics in reference [40]) to sample ion configurations and protein orientations, can be employed to compute, among other things, the electrostatic contribution to the potential of mean force between two protein molecules at a given distance and orientation in an electrolyte solution. The results of a series of test calculations on systems ranging from very simple to realistic solute molecules are presented here to demonstrate the quality and the feasibility of the novel BEM method.

Notice that throughout this paper, SI units are used.

2. Theory

2.1. Formulation of integral equations

The derivations in this Section follow very similar procedures as in reference [17]. Therefore, only the main results are given here.

Consider the case of two polarizable regions A and B at a given distance and orientation with respect to each other, immersed in a polarizable region S. All three regions contain free charges. All regions behave as linear dielectrics. The dielectric properties of this system are contained in the following set of equations.

$$\nabla^2 F(\mathbf{r},\mathbf{s}) = -\delta(\mathbf{r}-\mathbf{s}), \tag{1}$$

$$F(\mathbf{r},\mathbf{s}) = \frac{1}{4\pi|\mathbf{r}-\mathbf{s}|}, \tag{2}$$

$$\nabla^2 \varphi_{\mathrm{A}}(\mathbf{r}) = -\sum_i \frac{q_i^{\mathrm{A}}}{\epsilon_0 \epsilon_{\mathrm{A}}} \delta(\mathbf{r}-\mathbf{r}_i), \tag{3}$$

$$\nabla^2 \varphi_{\mathrm{B}}(\mathbf{r}) = -\sum_j \frac{q_j^{\mathrm{B}}}{\epsilon_0 \epsilon_{\mathrm{B}}} \delta(\mathbf{r}-\mathbf{r}_j), \tag{4}$$

$$\nabla^2 \varphi_{\mathrm{S}}(\mathbf{r}) = -\sum_k \frac{q_k^{\mathrm{S}}}{\epsilon_0 \epsilon_{\mathrm{S}}} \delta(\mathbf{r}-\mathbf{r}_k). \tag{5}$$

Here, ϵ_{A}, ϵ_{B} and ϵ_{S} are the dielectric constants of A, B and S, respectively, and q_i^{A}, q_j^{B} and q_k^{S} refer to the free charges of A, B and S, respectively. $F(\mathbf{r},\mathbf{s})$ with singularity in $\mathbf{s}$ is the fundamental solution of Eqs. (3)–(5) and satisfies Eq. (1). The functions φ_{A}, φ_{B} and φ_{S} are the electrostatic potentials in A, B and S, respectively. Eqs. (3) to (5) correspond to the Poisson equations for these regions. The potential φ_{S} in the solvent satisfies regularity conditions at infinity, i.e. $|\mathbf{r}|\varphi_{\mathrm{S}}(\mathbf{r})$ and $|\mathbf{r}|^2\nabla\varphi_{\mathrm{S}}(\mathbf{r})$ are bounded for $\mathbf{r}$ tending to infinity, so that the set of Eqs. (1) to (5) results in a unique solution to the problem.

The following boundary conditions apply at $\mathbf{r}_0$ on the surface Σ_{A} of A

$$\varphi_{\mathrm{A}}(\mathbf{r}_0) = \varphi_{\mathrm{S}}(\mathbf{r}_0), \tag{6}$$

$$\frac{\partial \varphi_{\mathrm{A}}(\mathbf{r}_0)}{\partial n_0} = \frac{\epsilon_{\mathrm{S}}}{\epsilon_{\mathrm{A}}} \frac{\partial \varphi_{\mathrm{S}}(\mathbf{r}_0)}{\partial n_0}, \tag{7}$$

where $\frac{\partial \varphi}{\partial n_0} = \nabla\varphi(\mathbf{r}_0)\cdot\mathbf{n}_0$ is the directional derivative of φ at $\mathbf{r}_0$ and $\mathbf{n}_0$ is the unit normal vector at $\mathbf{r}_0$ pointing outward (into the solvent region). Similarly, at $\mathbf{r}_0$ on the surface Σ_{B} of B, one has

$$\varphi_{\mathrm{B}}(\mathbf{r}_0) = \varphi_{\mathrm{S}}(\mathbf{r}_0), \tag{8}$$

$$\frac{\partial \varphi_{\mathrm{B}}(\mathbf{r}_0)}{\partial n_0} = \frac{\epsilon_{\mathrm{S}}}{\epsilon_{\mathrm{B}}} \frac{\partial \varphi_{\mathrm{S}}(\mathbf{r}_0)}{\partial n_0}. \tag{9}$$

This set of Eqs. (1) to (9) could describe two polarizable protein molecules immersed in an electrolyte solution. The latter is described in the present work as a collection of *explicit* charges in a background continuum. Notice that the free charges in S (the ions) are treated in exactly the same way as in regions A and B, that is, they are considered as point charges. Charge size is imposed, though, through the use of radii so that overlap between ions, for instance in the course of a simulation, is avoided. In fact this model for the ions corresponds to the primitive model of electrolytes, a theory known to predict the properties of electrolyte solutions very well at modest concentrations [39]. The classical Debye–Hückel theory for electrolyte solution expressed through the familiar linear PB equation, is *not* required here. The use of explicit ions significantly widens the applicability range of the present formulation with respect to previous formulations [17,7], which are based upon the linear PB equation.

Multiplying Eq. (2) with Eq. (3), subtracting φ_{A} times Eq. (1), with $\mathbf{s}\in\mathrm{A}$, and applying Green's second theorem to region A, one has for the potential at $\mathbf{r}_0^{\mathrm{A}}$ in A

$$\varphi_{\mathrm{A}}(\mathbf{r}_0^{\mathrm{A}}) = \int_{\Sigma_{\mathrm{A}}} \left(F(\mathbf{r}, \mathbf{r}_0^{\mathrm{A}}) \frac{\partial \varphi_{\mathrm{A}}(\mathbf{r})}{\partial n} - \varphi_{\mathrm{A}}(\mathbf{r}) \frac{\partial F(\mathbf{r}, \mathbf{r}_0^{\mathrm{A}})}{\partial n} \right) \mathrm{d}\sigma + \sum_i \frac{q_i^{\mathrm{A}}}{\epsilon_0 \epsilon_{\mathrm{A}}} F(\mathbf{r}_i, \mathbf{r}_0^{\mathrm{A}}). \tag{10}$$

Similarly,

$$\varphi_{\mathrm{B}}(\mathbf{r}_0^{\mathrm{B}}) = \int_{\Sigma_{\mathrm{B}}} \left(F(\mathbf{r}, \mathbf{r}_0^{\mathrm{B}}) \frac{\partial \varphi_{\mathrm{B}}(\mathbf{r})}{\partial n} - \varphi_{\mathrm{B}}(\mathbf{r}) \frac{\partial F(\mathbf{r}, \mathbf{r}_0^{\mathrm{B}})}{\partial n} \right) \mathrm{d}\sigma + \sum_j \frac{q_j^{\mathrm{B}}}{\epsilon_0 \epsilon_{\mathrm{B}}} F(\mathbf{r}_j, \mathbf{r}_0^{\mathrm{B}}) \tag{11}$$

and

$$\begin{aligned} \varphi_{\mathrm{S}}(\mathbf{r}_0^{\mathrm{S}}) = & \int_{\Sigma_{\mathrm{A}}} \left(-F(\mathbf{r}, \mathbf{r}_0^{\mathrm{S}}) \frac{\partial \varphi_{\mathrm{S}}(\mathbf{r})}{\partial n} + \varphi_{\mathrm{S}}(\mathbf{r}) \frac{\partial F(\mathbf{r}, \mathbf{r}_0^{\mathrm{S}})}{\partial n} \right) \mathrm{d}\sigma \\ & + \int_{\Sigma_{\mathrm{B}}} \left(-F(\mathbf{r}, \mathbf{r}_0^{\mathrm{S}}) \frac{\partial \varphi_{\mathrm{S}}(\mathbf{r})}{\partial n} + \varphi_{\mathrm{S}}(\mathbf{r}) \frac{\partial F(\mathbf{r}, \mathbf{r}_0^{\mathrm{S}})}{\partial n} \right) \mathrm{d}\sigma + \sum_k \frac{q_k^{\mathrm{S}}}{\epsilon_0 \epsilon_{\mathrm{S}}} F(\mathbf{r}_k, \mathbf{r}_0^{\mathrm{S}}). \end{aligned} \tag{12}$$

Here, the normal vector $\mathbf{n}$ at $\mathbf{r}$ on the surface of A or B always points into the solvent region.

We now express, the potentials in A, B and S as a function of the potentials $\varphi_{\mathrm{A}}(\mathbf{r})$ on Σ_{A} and $\varphi_{\mathrm{B}}(\mathbf{r})$ on Σ_{B} only, so that our first objective is to remove any reference to the directional derivatives $\frac{\partial \varphi_{\mathrm{A}}}{\partial n}$ and $\frac{\partial \varphi_{\mathrm{B}}}{\partial n}$ on the surfaces Σ_{A} and Σ_{B}.

From Eqs. (1), (2) and (5), with $\mathbf{s} \in \mathrm{A}$, and applying once more Green's second theorem to S, it is found that

$$\begin{aligned} & \int_{\Sigma_{\mathrm{A}}} \left(F(\mathbf{r}, \mathbf{r}_0^{\mathrm{A}}) \frac{\partial \varphi_{\mathrm{S}}(\mathbf{r}, \mathbf{r}_0^{\mathrm{A}})}{\partial n} - \varphi_{\mathrm{S}}(\mathbf{r}) \frac{\partial F(\mathbf{r}, \mathbf{r}_0^{\mathrm{A}})}{\partial n} \right) \mathrm{d}\sigma + \int_{\Sigma_{\mathrm{B}}} \left(F(\mathbf{r}, \mathbf{r}_0^{\mathrm{A}}) \frac{\partial \varphi_{\mathrm{S}}(\mathbf{r}, \mathbf{r}_0^{\mathrm{A}})}{\partial n} - \varphi_{\mathrm{S}}(\mathbf{r}) \frac{\partial F(\mathbf{r}, \mathbf{r}_0^{\mathrm{A}})}{\partial n} \right) \mathrm{d}\sigma \\ & - \sum_k \frac{q_k^{\mathrm{S}}}{\epsilon_0 \epsilon_{\mathrm{S}}} F(\mathbf{r}_k, \mathbf{r}_0^{\mathrm{A}}) = 0. \end{aligned} \tag{13}$$

Subtracting $\frac{\epsilon_{\mathrm{S}}}{\epsilon_{\mathrm{A}}}$ times Eq. (13) from Eq. (10) and using the boundary conditions, the electrostatic potential in A becomes

$$\begin{aligned} \varphi_{\mathrm{A}}(\mathbf{r}_0^{\mathrm{A}}) = & \left(\frac{\epsilon_{\mathrm{S}}}{\epsilon_{\mathrm{A}}} - 1 \right) \int_{\Sigma_{\mathrm{A}}} \frac{\partial F(\mathbf{r}, \mathbf{r}_0^{\mathrm{A}})}{\partial n} \varphi_{\mathrm{A}}(\mathbf{r}) \mathrm{d}\sigma - \frac{\epsilon_{\mathrm{S}}}{\epsilon_{\mathrm{A}}} \int_{\Sigma_{\mathrm{B}}} \left(F(\mathbf{r}, \mathbf{r}_0^{\mathrm{A}}) \frac{\epsilon_{\mathrm{B}}}{\epsilon_{\mathrm{S}}} \frac{\partial \varphi_{\mathrm{B}}(\mathbf{r})}{\partial n} - \varphi_{\mathrm{B}}(\mathbf{r}) \frac{\partial F(\mathbf{r}, \mathbf{r}_0^{\mathrm{A}})}{\partial n} \right) \mathrm{d}\sigma \\ & + \sum_i \frac{q_i^{\mathrm{A}}}{\epsilon_0 \epsilon_{\mathrm{A}}} F(\mathbf{r}_i, \mathbf{r}_0^{\mathrm{A}}) + \frac{\epsilon_{\mathrm{S}}}{\epsilon_{\mathrm{A}}} \sum_k \frac{q_k^{\mathrm{S}}}{\epsilon_0 \epsilon_{\mathrm{S}}} F(\mathbf{r}_k, \mathbf{r}_0^{\mathrm{A}}). \end{aligned} \tag{14}$$

From Eqs. (1), (2) and (4), with $\mathbf{s} \in \mathrm{A}$, and applying Green's second theorem to B, it is found that

$$\int_{\Sigma_{\mathrm{B}}} \left(F(\mathbf{r}, \mathbf{r}_0^{\mathrm{A}}) \frac{\partial \varphi_{\mathrm{B}}(\mathbf{r})}{\partial n} - \varphi_{\mathrm{B}}(\mathbf{r}) \frac{\partial F(\mathbf{r}, \mathbf{r}_0^{\mathrm{A}})}{\partial n} \right) \mathrm{d}\sigma + \sum_j \frac{q_j^{\mathrm{B}}}{\epsilon_0 \epsilon_{\mathrm{B}}} F(\mathbf{r}_j, \mathbf{r}_0^{\mathrm{A}}) = 0. \tag{15}$$

Adding $\frac{\epsilon_{\mathrm{B}} \epsilon_{\mathrm{S}}}{\epsilon_{\mathrm{S}} \epsilon_{\mathrm{A}}}$ times Eq. (15) to (14), the desired result is obtained.

$$\begin{aligned} \varphi_{\mathrm{A}}(\mathbf{r}_0^{\mathrm{A}}) = & \left(\frac{\epsilon_{\mathrm{S}}}{\epsilon_{\mathrm{A}}} - 1 \right) \int_{\Sigma_{\mathrm{A}}} \frac{\partial F(\mathbf{r}, \mathbf{r}_0^{\mathrm{A}})}{\partial n} \varphi_{\mathrm{A}}(\mathbf{r}) \mathrm{d}\sigma + \left(\frac{\epsilon_{\mathrm{S}}}{\epsilon_{\mathrm{A}}} - \frac{\epsilon_{\mathrm{B}}}{\epsilon_{\mathrm{A}}} \right) \int_{\Sigma_{\mathrm{B}}} \frac{\partial F(\mathbf{r}, \mathbf{r}_0^{\mathrm{A}})}{\partial n} \varphi_{\mathrm{B}}(\mathbf{r}) \mathrm{d}\sigma + \sum_i \frac{q_i^{\mathrm{A}}}{\epsilon_0 \epsilon_{\mathrm{A}}} F(\mathbf{r}_i, \mathbf{r}_0^{\mathrm{A}}) \\ & + \frac{\epsilon_{\mathrm{B}} \epsilon_{\mathrm{S}}}{\epsilon_{\mathrm{S}} \epsilon_{\mathrm{A}}} \sum_j \frac{q_j^{\mathrm{B}}}{\epsilon_0 \epsilon_{\mathrm{B}}} F(\mathbf{r}_j, \mathbf{r}_0^{\mathrm{A}}) + \frac{\epsilon_{\mathrm{S}}}{\epsilon_{\mathrm{A}}} \sum_k \frac{q_k^{\mathrm{S}}}{\epsilon_0 \epsilon_{\mathrm{S}}} F(\mathbf{r}_k, \mathbf{r}_0^{\mathrm{A}}). \end{aligned} \tag{16}$$

Notice that if there is no molecule B and the solvent is charge free with zero ionic strength, this equation becomes identical to Eq. (2.25) in reference [17]. The potential in A is seen to have a contribution from all charges (the summation terms) and a contribution from the boundaries (the surface integrals).

If the same procedure is repeated but now with molecule B instead of Eq. (16), one has for the potential in B

$$\varphi_{\mathrm{B}}(\mathbf{r}_0^{\mathrm{B}}) = \left(\frac{\epsilon_{\mathrm{S}}}{\epsilon_{\mathrm{B}}} - 1\right)\int_{\Sigma_{\mathrm{B}}} \frac{\partial F(\mathbf{r},\mathbf{r}_0^{\mathrm{B}})}{\partial n}\varphi_{\mathrm{B}}(\mathbf{r})\mathrm{d}\sigma + \left(\frac{\epsilon_{\mathrm{S}}}{\epsilon_{\mathrm{B}}} - \frac{\epsilon_{\mathrm{A}}}{\epsilon_{\mathrm{B}}}\right)\int_{\Sigma_{\mathrm{A}}} \frac{\partial F(\mathbf{r},\mathbf{r}_0^{\mathrm{B}})}{\partial n}\varphi_{\mathrm{A}}(\mathbf{r})\mathrm{d}\sigma + \frac{\epsilon_{\mathrm{A}}\epsilon_{\mathrm{S}}}{\epsilon_{\mathrm{S}}\epsilon_{\mathrm{B}}}\sum_i \frac{q_i^{\mathrm{A}}}{\epsilon_0\epsilon_{\mathrm{A}}}F(\mathbf{r}_i,\mathbf{r}_0^{\mathrm{B}}) + \sum_j \frac{q_j^{\mathrm{B}}}{\epsilon_0\epsilon_{\mathrm{B}}}F(\mathbf{r}_j,\mathbf{r}_0^{\mathrm{B}}) + \frac{\epsilon_{\mathrm{S}}}{\epsilon_{\mathrm{B}}}\sum_k \frac{q_k^{\mathrm{S}}}{\epsilon_0\epsilon_{\mathrm{S}}}F(\mathbf{r}_k,\mathbf{r}_0^{\mathrm{B}}). \tag{17}$$

From Eqs. (1)–(3), with $\mathbf{s}\in \mathrm{S}$, one can derive in the same way, for region A

$$\int_{\Sigma_{\mathrm{A}}}\left(F(\mathbf{r},\mathbf{r}_0^{\mathrm{S}})\frac{\partial\varphi_{\mathrm{A}}(\mathbf{r})}{\partial n} - \varphi_A(\mathbf{r})\frac{\partial F(\mathbf{r},\mathbf{r}_0^{\mathrm{S}})}{\partial n}\right)\mathrm{d}\sigma + \sum_i \frac{q_i^{\mathrm{A}}}{\epsilon_0\epsilon_{\mathrm{A}}}F(\mathbf{r}_i,\mathbf{r}_0^{\mathrm{S}}) = 0 \tag{18}$$

and also, from Eqs. (4), (1) and (2), with $\mathbf{s}\in \mathrm{S}$, for region B

$$\int_{\Sigma_{\mathrm{B}}}\left(F(\mathbf{r},\mathbf{r}_0^{\mathrm{S}})\frac{\partial\varphi_{\mathrm{B}}(\mathbf{r})}{\partial n} - \varphi_B(\mathbf{r})\frac{\partial F(\mathbf{r},\mathbf{r}_0^{\mathrm{S}})}{\partial n}\right)\mathrm{d}\sigma + \sum_j \frac{q_j^{\mathrm{B}}}{\epsilon_0\epsilon_{\mathrm{B}}}F(\mathbf{r}_j,\mathbf{r}_0^{\mathrm{S}}) = 0. \tag{19}$$

Adding $\frac{\epsilon_{\mathrm{A}}}{\epsilon_{\mathrm{S}}}$ times Eq. (18) and $\frac{\epsilon_{\mathrm{B}}}{\epsilon_{\mathrm{S}}}$ times Eqs. (19) to (12), one obtains for the electrostatic potential in S

$$\varphi_{\mathrm{S}}(\mathbf{r}_0^{\mathrm{S}}) = \left(1 - \frac{\epsilon_{\mathrm{A}}}{\epsilon_{\mathrm{S}}}\right)\int_{\Sigma_{\mathrm{A}}} \frac{\partial F(\mathbf{r},\mathbf{r}_0^{\mathrm{S}})}{\partial n}\varphi_{\mathrm{A}}(\mathbf{r})\mathrm{d}\sigma + \left(1 - \frac{\epsilon_{\mathrm{B}}}{\epsilon_{\mathrm{S}}}\right)\int_{\Sigma_{\mathrm{B}}} \frac{\partial F(\mathbf{r},\mathbf{r}_0^{\mathrm{S}})}{\partial n}\varphi_{\mathrm{B}}(\mathbf{r})\mathrm{d}\sigma + \frac{\epsilon_{\mathrm{A}}}{\epsilon_{\mathrm{S}}}\sum_i \frac{q_i^{\mathrm{A}}}{\epsilon_0\epsilon_{\mathrm{A}}}F(\mathbf{r}_j,\mathbf{r}_0^{\mathrm{S}}) + \frac{\epsilon_{\mathrm{B}}}{\epsilon_{\mathrm{S}}}\sum_j \frac{q_j^{\mathrm{B}}}{\epsilon_0\epsilon_{\mathrm{B}}}F(\mathbf{r}_i,\mathbf{r}_0^{\mathrm{S}}) + \sum_k \frac{q_k^{\mathrm{S}}}{\epsilon_0\epsilon_{\mathrm{S}}}F(\mathbf{r}_k,\mathbf{r}_0^{\mathrm{S}}). \tag{20}$$

Notice that if the solvent is charge free with zero ionic strength and there is just one molecule (A or B) in the solvent S, Eq. (20) becomes identical to Eq. (2.26) in reference [17].

Eqs. (16), (17) and (20) demonstrate that the electrostatic potential in any point can be expressed as a function of just two unknowns, φ_{A} on Σ_{A} and φ_{B} on Σ_{B}. We now seek two integral equations for φ_{A} and φ_{B} valid on Σ_{A} and Σ_{B}.

Taking the limits $\mathbf{r}_0^{\mathrm{A}} \to \Sigma_{\mathrm{A}}$ and $\mathbf{r}_0^{\mathrm{B}} \to \Sigma_{\mathrm{B}}$ in Eqs. (10) and (11), it is found that

$$\frac{1}{2}\varphi_{\mathrm{A}}(\mathbf{r}_0) = \int_{\Sigma_{\mathrm{A}}}\left(F(\mathbf{r},\mathbf{r}_0)\frac{\partial\varphi_{\mathrm{A}}(\mathbf{r})}{\partial n} - \varphi_{\mathrm{A}}(\mathbf{r})\frac{\partial F(\mathbf{r},\mathbf{r}_0)}{\partial n}\right)\mathrm{d}\sigma + \sum_i \frac{q_i^{\mathrm{A}}}{\epsilon_0\epsilon_{\mathrm{A}}}F(\mathbf{r}_i,\mathbf{r}_0). \tag{21}$$

$$\frac{1}{2}\varphi_{\mathrm{B}}(\mathbf{r}_0) = \int_{\Sigma_{\mathrm{B}}}\left(F(\mathbf{r},\mathbf{r}_0)\frac{\partial\varphi_{\mathrm{B}}(\mathbf{r})}{\partial n} - \varphi_{\mathrm{B}}(\mathbf{r})\frac{\partial F(\mathbf{r},\mathbf{r}_0)}{\partial n}\right)\mathrm{d}\sigma + \sum_j \frac{q_j^{\mathrm{B}}}{\epsilon_0\epsilon_{\mathrm{B}}}F(\mathbf{r}_j,\mathbf{r}_0), \tag{22}$$

where $\mathbf{r}_0 \in \sum_{\mathrm{A}}$ in Eq. (21) and $\mathbf{r}_0 \in \sum_{\mathrm{B}}$ in Eq. (22).

Taking the limit $\mathbf{r}_0^{\mathrm{S}} \to \Sigma_{\mathrm{A}}$ in Eq. (12) gives

$$\frac{1}{2}\varphi_{\mathrm{S}}(\mathbf{r}_0) = \int_{\Sigma_{\mathrm{A}}}\left(-F(\mathbf{r},\mathbf{r}_0)\frac{\partial\varphi_{\mathrm{S}}(\mathbf{r})}{\partial n} + \varphi_{\mathrm{S}}(\mathbf{r})\frac{\partial F(\mathbf{r},\mathbf{r}_0)}{\partial n}\right)\mathrm{d}\sigma + \int_{\Sigma_{\mathrm{B}}}\left(-F(\mathbf{r},\mathbf{r}_0)\frac{\partial\varphi_{\mathrm{S}}(\mathbf{r})}{\partial n} + \varphi_{\mathrm{S}}(\mathbf{r})\frac{\partial F(\mathbf{r},\mathbf{r}_0)}{\partial n}\right)\mathrm{d}\sigma + \sum_k \frac{q_k^{\mathrm{S}}}{\epsilon_0\epsilon_{\mathrm{S}}}F(\mathbf{r}_k,\mathbf{r}_0), \tag{23}$$

where $\mathbf{r}_0 \in \Sigma_{\mathrm{A}}$. Adding Eq. (21) and $\frac{\epsilon_{\mathrm{S}}}{\epsilon_{\mathrm{A}}}$ times Eq. (23) and using the boundary conditions, it follows for the potential $\varphi_{\mathrm{A}}(\mathbf{r}_0)$ on Σ_{A} that

$$\frac{1}{2}\left(1 + \frac{\epsilon_{\mathrm{S}}}{\epsilon_{\mathrm{A}}}\right)\varphi_{\mathrm{A}}(\mathbf{r}_0) = \left(\frac{\epsilon_{\mathrm{S}}}{\epsilon_{\mathrm{A}}} - 1\right)\int_{\Sigma_{\mathrm{A}}} \frac{\partial F(\mathbf{r},\mathbf{r}_0)}{\partial n}\varphi_{\mathrm{A}}(\mathbf{r})\mathrm{d}\sigma + \frac{\epsilon_{\mathrm{S}}}{\epsilon_{\mathrm{A}}}\int_{\Sigma_{\mathrm{B}}}\left(-F(\mathbf{r},\mathbf{r}_0)\frac{\epsilon_{\mathrm{B}}}{\epsilon_{\mathrm{S}}}\frac{\partial\varphi_{\mathrm{B}}(\mathbf{r})}{\partial n} + \varphi_{\mathrm{B}}(\mathbf{r})\frac{\partial F(\mathbf{r},\mathbf{r}_0)}{\partial n}\right)\mathrm{d}\sigma + \sum_i \frac{q_i^{\mathrm{A}}}{\epsilon_0\epsilon_{\mathrm{A}}}F(\mathbf{r}_i,\mathbf{r}_0) + \frac{\epsilon_{\mathrm{S}}}{\epsilon_{\mathrm{A}}}\sum_k \frac{q_k^{\mathrm{S}}}{\epsilon_0\epsilon_{\mathrm{S}}}F(\mathbf{r}_k,\mathbf{r}_0). \tag{24}$$

Finally, taking the limit $\mathbf{r}_0^{\mathrm{A}} \to \Sigma_{\mathrm{A}}$ in Eq. (15), multiplying the result with $\frac{\epsilon_{\mathrm{B}}\epsilon_{\mathrm{S}}}{\epsilon_{\mathrm{S}}\epsilon_{\mathrm{A}}}$ and adding this to Eq. (24), gives

$$\frac{1}{2}\left(1+\frac{\epsilon_S}{\epsilon_A}\right)\varphi_A(\mathbf{r}_0)=\left(\frac{\epsilon_S}{\epsilon_A}-1\right)\int_{\Sigma_A}\frac{\partial F(\mathbf{r},\mathbf{r}_0)}{\partial n}\varphi_A(\mathbf{r})d\sigma+\left(\frac{\epsilon_S}{\epsilon_A}-\frac{\epsilon_B}{\epsilon_A}\right)\int_{\Sigma_B}\frac{\partial F(\mathbf{r},\mathbf{r}_0)}{\partial n}\varphi_B(\mathbf{r})d\sigma$$
$$+\sum_i\frac{q_i^A}{\epsilon_0\epsilon_A}F(\mathbf{r}_i,\mathbf{r}_0)+\frac{\epsilon_B\epsilon_S}{\epsilon_S\epsilon_A}\sum_j\frac{q_j^B}{\epsilon_0\epsilon_B}F(\mathbf{r}_j,\mathbf{r}_0)+\frac{\epsilon_S}{\epsilon_A}\sum_k\frac{q_k^S}{\epsilon_0\epsilon_S}F(\mathbf{r}_k,\mathbf{r}_0). \quad (25)$$

Notice that if the solvent S is charge free and there is no molecule B, this equation becomes identical to Eq. (2.24) in reference [17].

Following similar steps, one finds that

$$\frac{1}{2}\left(1+\frac{\epsilon_S}{\epsilon_B}\right)\varphi_B(\mathbf{r}_0)=\left(\frac{\epsilon_S}{\epsilon_B}-1\right)\int_{\Sigma_B}\frac{\partial F(\mathbf{r},\mathbf{r}_0)}{\partial n}\varphi_B(\mathbf{r})d\sigma+\left(\frac{\epsilon_S}{\epsilon_B}-\frac{\epsilon_A}{\epsilon_B}\right)\int_{\Sigma_A}\frac{\partial F(\mathbf{r},\mathbf{r}_0)}{\partial n}\varphi_A(\mathbf{r})d\sigma$$
$$+\frac{\epsilon_A\epsilon_S}{\epsilon_S\epsilon_B}\sum_i\frac{q_i^A}{\epsilon_0\epsilon_A}F(\mathbf{r}_i,\mathbf{r}_0)+\sum_j\frac{q_j^B}{\epsilon_0\epsilon_B}F(\mathbf{r}_j,\mathbf{r}_0)+\frac{\epsilon_S}{\epsilon_B}\sum_k\frac{q_k^S}{\epsilon_0\epsilon_S}F(\mathbf{r}_k,\mathbf{r}_0). \quad (26)$$

Eqs. (25) and (26) represent a pair of integral equations for φ_A and φ_B valid on the surfaces Σ_A and Σ_B.

Notice that, from Eqs. (25, 26), if $\epsilon_A=\epsilon_B=\epsilon_S=\epsilon$, both the potential on A and B correspond to the regular Coulomb potential, but screened by a factor ϵ, as expected.

2.2. Electrostatic energy

The total electrostatic energy of a system consisting of two molecules A and B in a electrolyte solution with explicit ions is given from

$$W_{el}=\frac{1}{2}\sum_l q_l\varphi(\mathbf{r}_l)=\frac{1}{2}\sum_i q_i^A\varphi_A(\mathbf{r}_i)+\frac{1}{2}\sum_j q_j^B\varphi_B(\mathbf{r}_j)+\frac{1}{2}\sum_k q_k^S\varphi_S(\mathbf{r}_k)=W_{el}^{(q)}+W_{el}^{(b)}, \quad (27)$$

where q_l is one of the charges in the system and $\varphi(\mathbf{r}_l)$ is the *total* potential at the charge location $\mathbf{r}_l$. The total electrostatic potential is determined from Eqs. (16), (17) and (20) and includes the effects of mutual polarization between the different regions in the system. Eq. (27) is appropriate for linear dielectric media [13]. The total potential $\varphi(\mathbf{r})$ has a contribution $\varphi^{(q)}(\mathbf{r})$ from all charges and a contribution $\varphi^{(b)}(\mathbf{r})$ from the boundaries, so that the total electrostatic energy is the sum of a contribution $W_{el}^{(q)}$ due to interactions between all charges, represented by the summation terms of Eqs. (16), (17) and (20), and a contribution $W_{el}^{(b)}$ due to interactions of charges with the boundaries, represented by the integrals terms of Eqs. (16), (17) and (20). The calculation of $W_{el}^{(b)}$ generally involves a numerical integration over the boundaries [17,7].

$W_{el}^{(q)}$ corresponds to Coulomb-like interactions according to

$$W_{el}^{(q)}=\frac{1}{2\epsilon_A}\sum_{p,i}\frac{q_p^Aq_i^A}{\epsilon_0|\mathbf{r}_i-\mathbf{r}_p|}+\frac{1}{2\epsilon_A}\sum_{p,j}\frac{q_p^Aq_j^B}{\epsilon_0|\mathbf{r}_j-\mathbf{r}_p|}+\frac{1}{2\epsilon_A}\sum_{p,k}\frac{q_p^Aq_k^S}{\epsilon_0|\mathbf{r}_k-\mathbf{r}_p|}+\frac{1}{2\epsilon_B}\sum_{q,i}\frac{q_q^Bq_i^A}{\epsilon_0|\mathbf{r}_i-\mathbf{r}_q|}+\frac{1}{2\epsilon_B}\sum_{q,j}\frac{q_q^Bq_j^B}{\epsilon_0|\mathbf{r}_j-\mathbf{r}_q|}$$
$$+\frac{1}{2\epsilon_B}\sum_{q,k}\frac{q_q^Bq_k^S}{\epsilon_0|\mathbf{r}_k-\mathbf{r}_q|}+\frac{1}{2\epsilon_S}\sum_{r,i}\frac{q_r^Sq_i^A}{\epsilon_0|\mathbf{r}_i-\mathbf{r}_r|}+\frac{1}{2\epsilon_S}\sum_{r,j}\frac{q_r^Sq_j^B}{\epsilon_0|\mathbf{r}_j-\mathbf{r}_r|}+\frac{1}{2\epsilon_S}\sum_{r,k}\frac{q_r^Sq_k^S}{\epsilon_0|\mathbf{r}_k-\mathbf{r}_r|}. \quad (28)$$

It is seen that the cross-terms (direct interaction between charges in *different* regions) do *not* symmetrically contribute to the total electrostatic energy, because of different prefactors $\frac{1}{\epsilon_A}$, $\frac{1}{\epsilon_B}$ and $\frac{1}{\epsilon_S}$. The terms on the diagonal (interactions between charges in the *same* region) can be converted according to $\frac{1}{2}\sum_n\sum_m=\sum_{n<m}$ and are the conventional intramolecular (intrasolvent) interactions that also appear (except for the intrasolvent part) in the case of a single solute in a solvent without free charges [17,16]. Both $\varphi^{(q)}$ and $W_{el}^{(q)}$ can be computed by standard means.

2.3. Numerical solution of integral equations

Generally, the integral equations must be solved by numerical means. In this work, we employ a solution based upon the boundary element method (BEM). First the integral Eqs. (25), (26) are rewritten as

$$\frac{\epsilon_S+\epsilon_A}{2}\varphi_A(\mathbf{s}) = (\epsilon_S-\epsilon_A)\int_{\Sigma_A}\frac{\partial F(\mathbf{r},\mathbf{s})}{\partial n}\varphi_A(\mathbf{r})d\sigma + (\epsilon_S-\epsilon_B)\int_{\Sigma_B}\frac{\partial F(\mathbf{r},\mathbf{s})}{\partial n}\varphi_B(\mathbf{r})d\sigma + \sum_i \frac{q_i}{\epsilon_0}F(\mathbf{r}_i,\mathbf{s}), \tag{29}$$

$$\frac{\epsilon_S+\epsilon_B}{2}\varphi_B(\mathbf{t}) = (\epsilon_S-\epsilon_B)\int_{\Sigma_A}\frac{\partial F(\mathbf{r},\mathbf{t})}{\partial n}\varphi_A(\mathbf{r})d\sigma + (\epsilon_S-\epsilon_A)\int_{\Sigma_B}\frac{\partial F(\mathbf{r},\mathbf{t})}{\partial n}\varphi_A(\mathbf{r})d\sigma + \sum_i \frac{q_i}{\epsilon_0}F(\mathbf{r}_i,\mathbf{t}), \tag{30}$$

where the summation terms are over *all* charges of the solutes/solvent system and correspond to the Coulomb potential on the surfaces.

Following a notation similar to that in references [7,16,17], Eqs. (29, 30) are written as a single matrix equation (see Appendix A for some of the details)

$$(\mathbf{c}^T\mathbf{I}-\mathbf{S})\mathbf{x} = \mathbf{b}. \tag{31}$$

Here, the vector $\mathbf{x}$ of length n, where n is the number of collocation points on the boundaries, contains the unknown functions $(\epsilon_S-\epsilon_A)\varphi_A$ and $(\epsilon_S-\epsilon_B)\varphi_B$. $\mathbf{I}$ is a diagonal matrix, the vector $\mathbf{c}$ depends on values of the dielectric constants, $\mathbf{S}$ corresponds to the kernels of the form $\frac{\partial F(\mathbf{r},\mathbf{s})}{\partial n}$ in the integral equations, and the vector $\mathbf{b}$ corresponds to the source terms in Eqs. (29, 30). The exact form of the matrix elements of $\mathbf{S}$ depend on the details of the discretization or collocation method employed and the geometry of the boundaries, but not on the values of the dielectric constants. Eq. (31) can be solved for $\mathbf{x}$ with LU-decomposition techniques [41] or iterative procedures [42]. This work relies upon the LU-decomposition method.

The solution vector $\mathbf{x}$ is employed to numerically integrate over the boundaries to calculate the contribution $W_{el}^{(b)}$ to the electrostatic energy The integrals can be calculated along similar lines as the matrix elements of the matrix $\mathbf{S}$ are obtained (Appendix A). For instance, for the surface integrals of Eq. (16), it is found that [7]

$$\Phi^{(b)} = \frac{1}{\epsilon_A}\mathbf{Z}\mathbf{x}, \tag{32}$$

where the matrix $\mathbf{Z}$ represents the kernels of the form $\frac{\partial F(\mathbf{r},\mathbf{s})}{\partial n}$ in the surface integrals of Eq. (16) – see also Eqs. (55–59) in the Appendix. The vector $\Phi^{(b)}$ holds the contribution to the total potential due to the boundaries. The length of this vector is the number of points m in A where the potential $\varphi_A^{(b)}$ is to be calculated, so that $\mathbf{Z}$ has dimensions $m\times n$. The matrix $\mathbf{Z}$ depends on the positions of the charges inside A, the details of the collocation method, and the geometry of the boundaries.

2.4. Monte Carlo simulation

The above formulation gives the total electrostatic energy for a given configuration of one or two solutes in an electrolyte. In this work, this formulation is employed in Monte Carlo simulations of solutes in NaCl with concentrations ranging from 0.05 to 0.15 M, the latter being the salt concentration under physiological conditions. The simulations were performed in the canonical ensemble with importance sampling [43]. A trial move of a ion consisted of placing it at a random position somewhere in the box. A trial move of a solute molecule consisted of a random translation followed by a random rotation, where the rotation matrix is computed from a quaternion formalism [44,45]. The energy difference is subsequently evaluated to test if the new configuration is representative for the system. The Monte Carlo energy includes a hard-sphere potential to avoid overlap between solute atoms and ions. Internal degrees of freedom for the solutes were ignored and, consequently, solute molecules act like rigid bodies. The temperature of the system was always 298 K, the dielectric constant of the solutes was always 4, and the dielectric constant of the solvent was always 80. The box dimensions were chosen such that at 0.15 M NaCl the distance between the solutes' surfaces and the edge of the box was at least 6.0 nm, resulting in several 100 of ions at 0.15 M. The box size was increased to simulate at lower ionic strength so as to avoid a difference in sampling frequencies. The simulations rely on periodic boundary conditions (PBC) with the nearest image approximation (NIA) [43]. The PBC + NIA approach is appropriate for simulations of electrolytes based upon the primitive model. The charge distribution of the solute was constant (that is, pH effects were not accounted for).

One test system was concerned with a very simple case of two spherical objects, each carrying a physical dipole parallel to the z-axis. The dipole was constructed from two charges of values -2 and $+2$ placed at a distance of 1 nm with respect to each other inside a sphere with a radius of 1 nm. The negative charge was

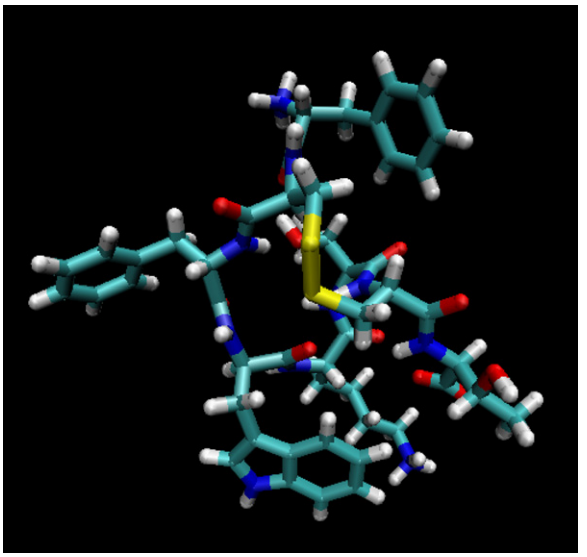

Fig. 1. Structure of the peptide sandostatin. This molecule consists of eight residues (Phe-Cys-Phe-Trp-Lys-Thr-Cys-Thr) and carries an overall positive charge of +1. A structure of the peptide was obtained from the PDB entry 1soc [54] and its charge distribution was obtained from the Gromacs force field [55]. There exists an disulphide bridge between the two Cys residues. The figure was obtained with visual molecular dynamics [56].

placed on the negative side of the z-axis. The distance between the spheres' centers of mass was 2.5 nm and was kept unchanged, while also the orientation of the spheres was fixed. The box size for this simulation was almost 21 nm and there were 812 ions in the system.

Three simulations of two peptides in 0.05, 0.10 and 0.15 M NaCl, respectively, were carried out as well. The peptide corresponded to sandostatin (a somatostatin analogue), a peptide hormone that we have used before [34,46]. This molecule consists of eight residues and carries an overall positive charge (some more details are given in the caption to Fig. 1). As indicated above, the total number of ions in these simulations was always the same (846), but the box size was appropriately adapted to obtain the required ionic strength (about 21, 24 and 30 nm for 0.15, 0.10 and 0.05 M NaCl, respectively). The two peptides were initially placed at a distance of 3 nm but otherwise were free to explore the whole of the box through rigid body motion (rotation and translation). Each simulation took about 10,000,000 steps. The peptide's triangulated surfaces were obtained as described in reference [47]. The matrix $\mathbf{S}$ is updated and consequently the LU-decomposition is carried out when the orientation of one of the solutes changes with respect to the other during a Monte Carlo step. The LU-decomposed matrix of the previous step is restored if the new state is not accepted.

3. Results

The quality of the boundary element method was considered by performing a simple test calculation on two spherical objects A and B, each containing a single charge q_A and q_B located at the center of a sphere with a radius of 1 nm. Fig. 2 displays the interaction energy with $q_A = +1$ and $q_B = -1$ in an solvent with *zero* ionic strength, as a function of the number of triangles of the spherical surfaces. The interaction energy $W_{el,\,int}$ at a given distance between the charges was computed simply as $W_{el,\,int}(A,B) = W_{el}(A,B) - W_{el}(A) - W_{el}(B)$, that is, as the difference of the total electrostatic energy of the combined system (A,B) and the sum of the total electrostatic energy of the individual systems (A and B). It is seen that with an increasing number of triangles, the numerical result quickly approaches the exact value. While this work does not present the best possible approach to numerically solve the integral equations, it appears to be of sufficient accuracy for the scope of this paper.

Fig. 3(a) shows the density (the *ratio* of the actual number density in parallel slabs and the bulk density, that is) of ions in the simulation box containing two spherical objects, each with a physical dipole parallel to the

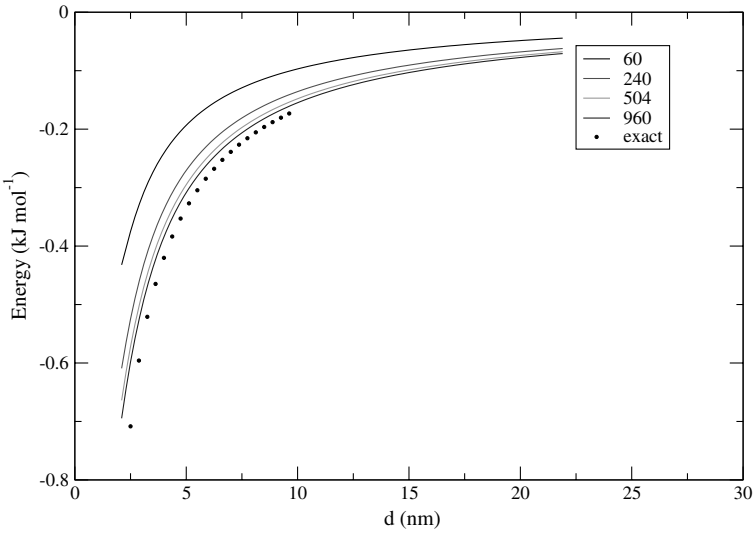

Fig. 2. Electrostatic interaction between two spherical objects (each with a radius of 1.0 nm), each containing a single charge (+1 and −1, respectively). The ionic strength is zero. The calculation is performed for an increasing number of boundary elements or triangles, ranging from 60 to 960 elements. The triangulated surface was obtained as described elsewhere [17]. The exact result is obtained from an implementation based upon reference [57], as kindly provided by Dr. Xueyu Song (Department of Chemistry, Iowa State University, Ames, IA 50011, USA).

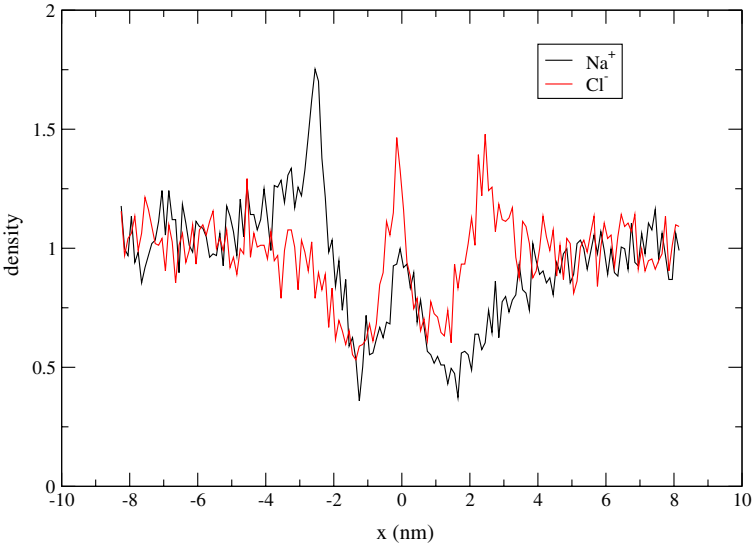

Fig. 3. Density of ions (Na^+ and Cl^-) throughout the simulation box parallel to the z-direction for the case of two physical dipoles, each inside a sphere with a radius of 1 nm. Each dipole was constructed from two charges with charge values −2 and +2 placed at a distance of 1 nm with respect to each other and placed on the negative and positive z-axis, respectively. The distance between the centers of the spheres was 2.5 nm. The graph displays the ratio of the density in slabs perpendicular to the z-axis and the bulk number density. The width of a slab in the z-direction was 0.1 nm, while the width of the slab perpendicular to the z-axis was 3.0 nm. If the latter had taken the full width of the simulation box, the inhomogeneity in the density would have been more difficult to observe. The relatively small size of the sphere with respect to the box sizes would have obscured the inhomogeneity of the density and the calculation would not have been sensitive enough to see the effects. This calculation method renders the graph noisier though.

z-axis. It is observed that, close to the spheres, there exists an inhomogeneity in the density, which is obviously due to the asymmetric charge distribution of the two spheres. On the negative z-axis there is an accumulation of positive ions (Na^+), while on the positive side, one observes the opposite, as one would expect. Since there is

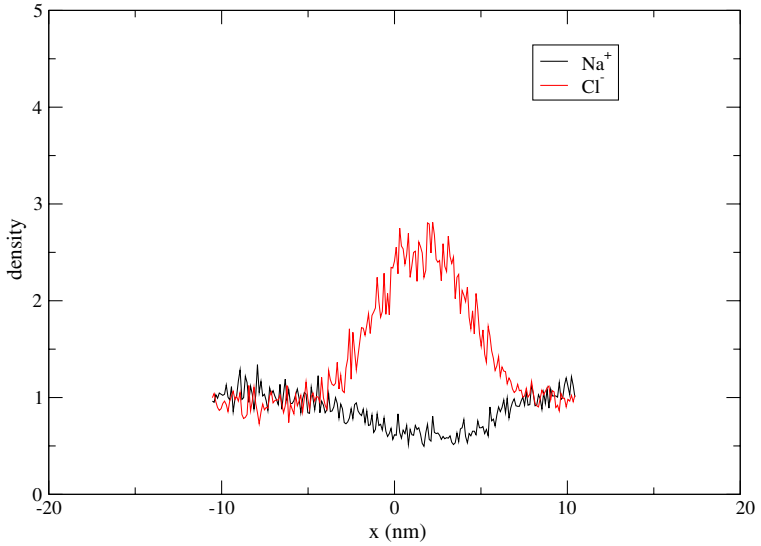

Fig. 4. Density of ions throughout the simulation box parallel to the x-direction for the case of two peptides (sandostatin) in a box. The box size was about 21 nm. The density is calculated in a similar manner as for Fig. 3.

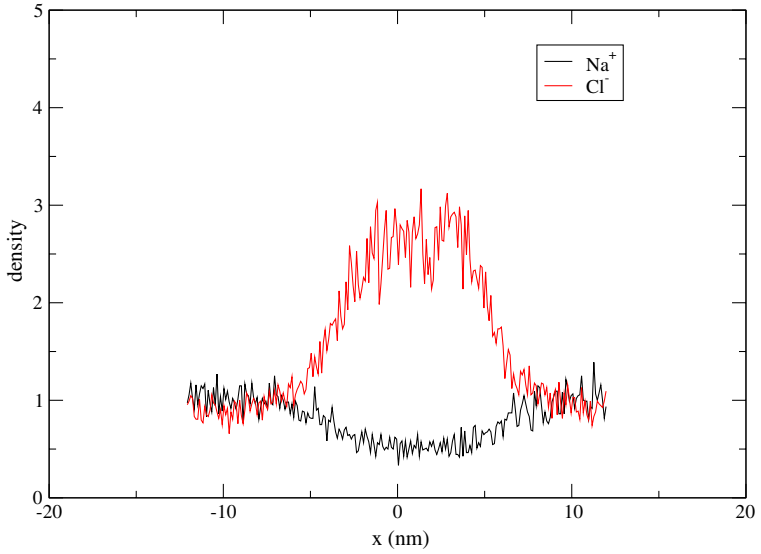

Fig. 5. As Fig. 4, but now the ionic strength is 0.10 M NaCl. The box size was about 24 nm.

space between the two spheres (0.5 nm), ions can enter that region and there appears to be an higher probability to observe a negative ion than a positive ion in that region. Towards the edges of the box, the density approaches the bulk value (the ratio of the actual number density in slabs and bulk density approaches 1). Due to the hard-sphere potential between the ions and spheres, ions were not allowed to enter the region inside the spheres.

We also performed a number of Monte Carlo simulations of a system consisting of two peptides. Figs. 4–6 show the distribution of ions throughout the box for these simulations. Since the peptides carry an overall positive charge, there is a tendency of negative Cl^- ions to occupy the regions around the peptides. It is observed that the density of $Cl^-(Na^+)$ ions with respect to the bulk density in between the two peptides is increasing (decreasing) with decreasing ionic strength. Further away from the peptides, towards the box edges, the ion density reaches the bulk value, as it should. The peptides are free to roam the entire simulation box and

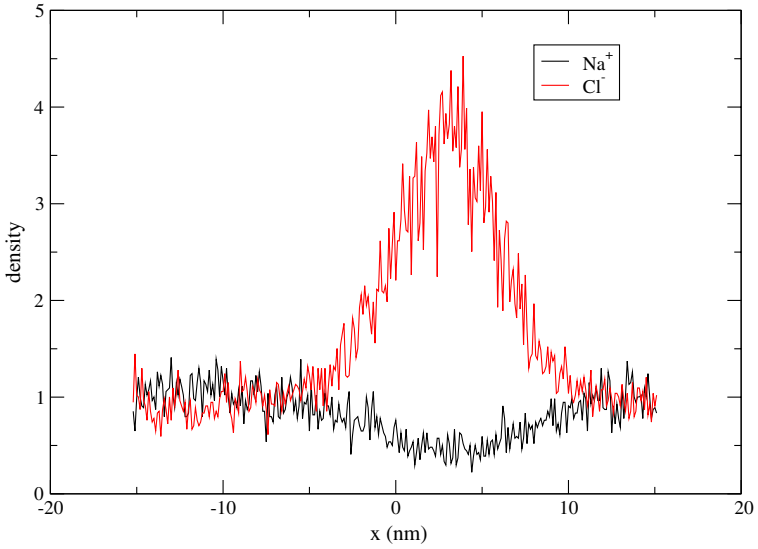

Fig. 6. As Fig. 4, but now the ionic strength is 0.05 M NaCl. The box size was about 30 nm.

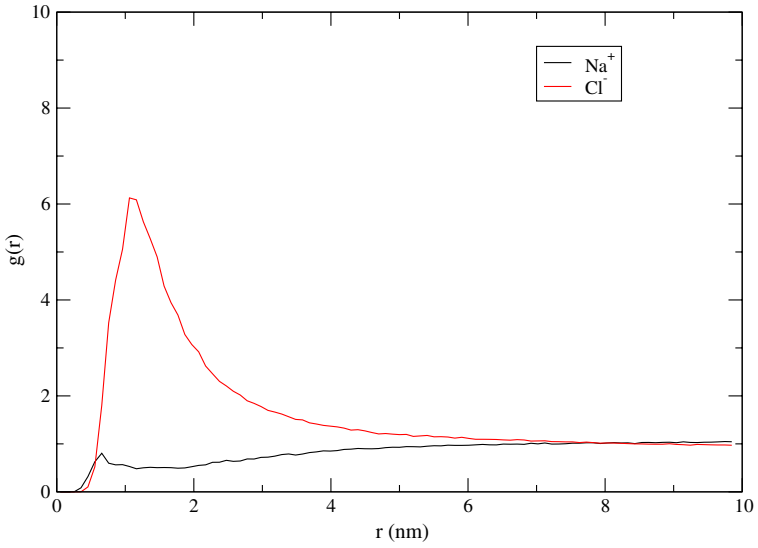

Fig. 7. The radial distribution function $g(r)$ of ions around the peptides at 0.15 M NaCl.

from the Figures, it is observed that they occupy mostly the region between about −5 to +10 nm. Much longer simulations would better cover the rest of the box, though.

Figs. 7–9 display the radial distribution function $g(r)$ of ions with respect to the centers of mass of the peptides, averaged over the orientations of the peptides (an analysis of the orientation of the peptides with respect to each other over the full course of the simulation indicated no particular preference). With decreasing ionic strength, the spatial correlation between the positive peptides and the ions is longer ranged, but disappears at a distance of 8 to 10 nm. This is in correspondence with Figs. 4–6 and indicates that the number density of ions approaches the bulk value beyond, say, 10 nm on either side of the middle of the box. Note also that Figs. 7–9 possibly indicate a degree of penetration of ions into the outer regions of the peptides, as the *radius* of the peptides is about 1 nm. The distribution of ions around the peptides in a way follows that of an electric double layer as is observed at a charged surface [34]. With decreasing ionic strength, a stronger accumulation of Cl^-

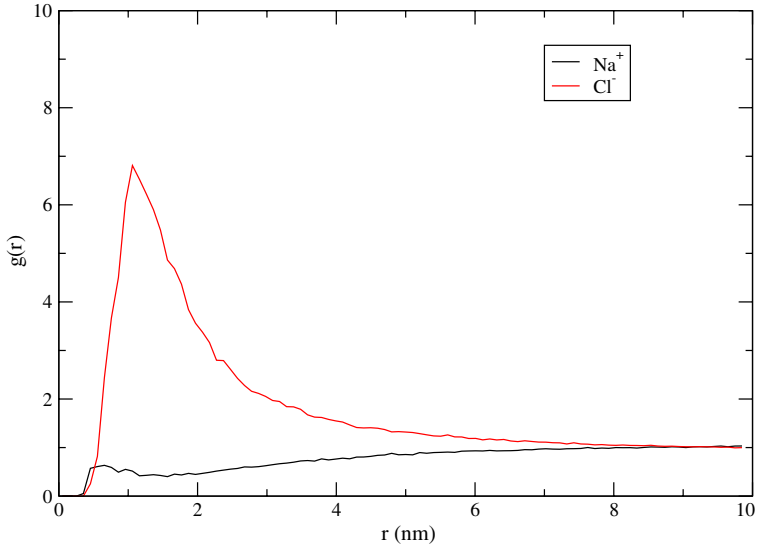

Fig. 8. As Fig. 7, but now the ionic strength is 0.10 M NaCl.

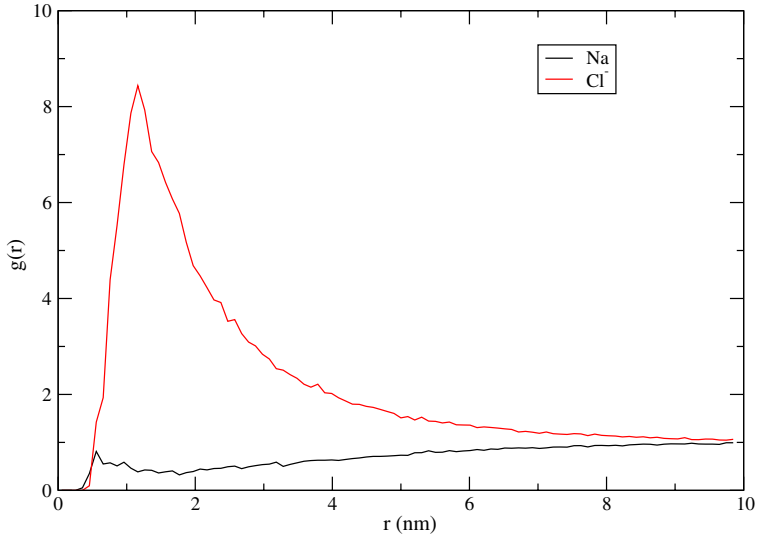

Fig. 9. As Fig. 7, but now the ionic strength is 0.05 M NaCl.

ions is observed at the surfaces of the peptides at about $r = 1$ nm. The peptide is, however, far from spherical (Fig. 1) and it is therefore quite possible that, in one region at the peptide's surface, the ions are closer to the peptide's center of mass than in another region.

Fig. 10 shows the radial distribution function between Na^+ and Cl^- for the three solute simulations. These results also suggest an increased spatial correlation at lower ionic strengths due to reduced screening effects. At the same time, due to a stronger average interaction between the ions, a stronger accumulation of counter charges is observed at the ion surfaces. Descriptions based upon a full continuum description of electrolytes do not account for explicit ion–ion correlation.

Finally, in Fig. 11, the frequency plot of the distance between the two peptides is shown. This is a measure for the potential of mean force. For 0.15 and 0.10 M NaCl, the distances most often visited appear to be in the range of 6–8 nm. For 0.05 M NaCl there is a considerable degree of sampling of shorter distances, while the

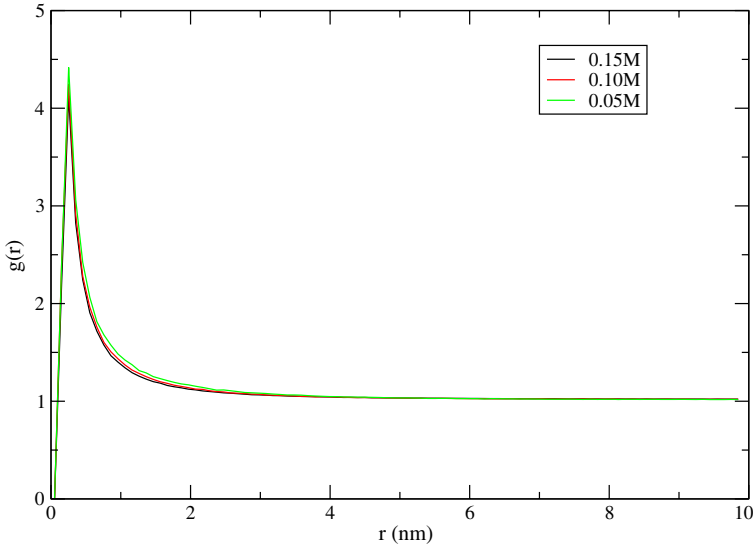

Fig. 10. The radial distribution function between ions at 0.15 M, 0.10 M and 0.05 M NaCl.

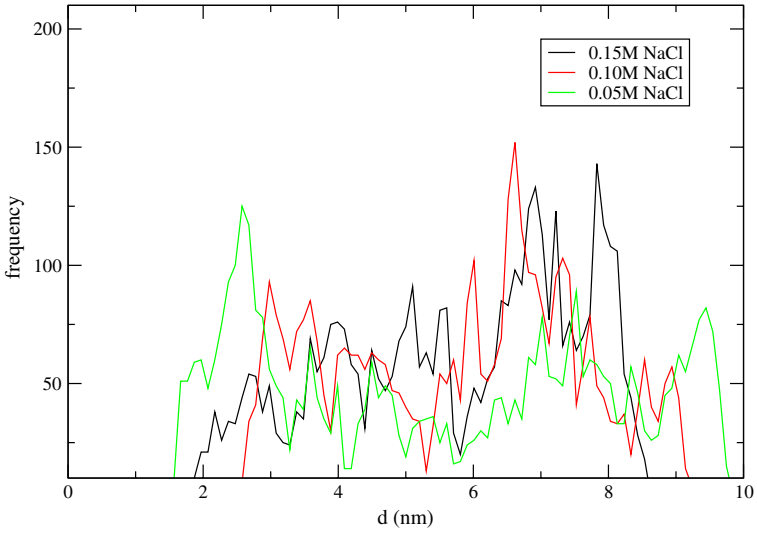

Fig. 11. A frequency plot of the distance between the sandostatin peptide molecules at 0.15 M, 0.10 M and 0.05 M NaCl.

system also visits distances beyond 8 nm. Generally, with decreasing ionic strength, the region beyond 8 nm is more frequently visited, while there also seems to be an increasing tendency to visit shorter distances more often.

4. Discussion

This work presents a novel formulation to describe ionic strength in a boundary element method scheme for the calculation of electrostatic interactions in and between proteins. Without exception, current formulations that include mutual polarization effects and ionic strength depend on a full continuum model limiting their applicability and validity range. One advantage of the usage of explicit ions is that the present formulation is not limited at all to 1:1 electrolytes. It is straightforward to apply the approach to asymmetric electrolytes such as $CaCl_2$, a realm of applications where the standard Poisson–Boltzmann utterly fails [39]. Another

advantage is concerned with the details of interactions between charged groups of the solute and the solvent, which in a full continuum description are totally incorrectly described, therefore, interfering with the dynamical properties of these groups.

Many researchers, in the 1980–1990's, have already commented on the importance of ion–ion correlation in describing the physical properties of electrolyte solutions [39]. This is probably best reflected in the (mean) activity coefficient γ, which appears in the chemical potential, a free energy. Its dependence on the ionic strength predicts a straight line according the Debye–Hückel theory ($-ln\gamma$ versus the square root of the ionic strength), which in fact is not the case at increasingly higher ionic strengths. The predicted dependence is true only at very low concentrations. Computer simulations using an explicit model of ions in a continuum background and recent statistical mechanical theories reproduce the correct behaviour of γ quite well. Deviations are expected and are also observed in experiments with concentrations above about 0.01 mol l^{-1}, although each salt has its own peculiarities. The fact is that methods based upon an explicit treatment of ions describe the thermodynamical and structural properties of electrolytes better. As it is true that the solvent very much influences the structural and other properties of a protein [48], one can argue that a pure continuum model for the solvent is too crude to properly simulate proteins in electrolyte solutions.

The feasibility and the correctness of the present formulation has been demonstrated by a number of test calculations. A typical outcome for the electrostatic interaction between two proteins in an electrolyte solution is presented in Fig. 11. Generally, this figure suggests that with decreasing ionic strength, the region beyond 8 nm is more often visited. There also appears to be an increasing tendency to visit more often shorter distances. The fact that the system visits longer distances is a consequence of reduced screening at lower ionic strengths, rendering the repulsive interaction stronger due to the overall positive charge of the peptide. Fig. 1 shows that the molecule is strongly asymmetric. It contains two widely separated positive charges located on the N-terminus and the Lys residue, and there is a negative charge on the C-terminus of the peptide positioned in about the same region as the N-terminus. The molecules carry, therefore, a dipole and also higher order multipoles. At short distances between the two peptides, the details of the charge distribution and the peptide's structure will strongly affect the potential of mean force between the molecules. The electrostatic interaction is stronger at lower ionic strengths, resulting in a slightly higher probability of the two molecules sticking to each other. This is a consequence of the interaction between the dipoles and the other higher order multipoles of the two molecules, the effects of which are significantly reduced at longer distances where the monopole term dominates the potential of mean force, pushing them away from each other. At higher ionic strengths, these interactions are effectively screened; also at the shorter distances. A similar effect was observed previously [34].

A few practical notes are worth mentioning. While this work relied on the LU-decomposition method to solve the matrix equation Eq. (31), this method is not practical for large linear algebraic systems due to both memory and CPU speed limitations. So, for large macromolecular systems, an iterative procedure is usually employed to solve the matrix equation. The inclusion of ionic strength does not modify the size of the matrix $\mathbf{S}$. In implementations based upon the linear Poisson–Boltzmann equation, the size of this matrix doubles if ionic strength is included in the description [17]. This negatively affects both memory requirements and efficiency, if for instance a LU decomposition method is employed to solve the matrix equation. One could object against the use of explicit ions for reasons of efficiency when compared to pure continuum approaches, since additional computing time is now spent on the handling of explicit ions through a simulation scheme. On the other hand, any realistic simulation model should include some degree of flexibility for the solute. In the current approach, the number of ions (except for small solutes) is typically less than the number of protein atoms. Therefore, in any ensemble or dynamical simulation most of the computation time is now concerned with the energy and forces related the protein atoms, instead of with the solvent. This is to be contrasted with the case of an all-atom molecular dynamics simulation, where 80–90% of the computation time is concerned with the solvent. Then again, in the present formulation, it is necessary to regularly update the boundary of the solute molecules and also the matrix $\mathbf{S}$, because of the changing conformations of the proteins in the course of a simulation. Obviously this would reduce the efficiency of the method compared to *implicit* solvation models. The handling of the surface is not a major obstacle, since a number of very efficient algorithms already exists for this purpose (a short overview is presented in reference [47]). The calculation of the surface may in fact not be required at every step of the simulation. In conclusion then, when compared to an application of molecular

dynamics that relies on an implicit solvent model, the inclusion of explicit ions should not drastically decrease the efficiency of the simulation method and is certainly more efficient than an all atom model.

The Monte Carlo simulations rely on the simple PBC + NIA approximation (there are no cut-off distances in this scheme) to compute the direct screened Coulomb interaction between charges (Eq. (28)) and to calculate the right-hand side of the matrix equation (Eq. (31)). The results indicate that towards the edges of the simulation box, the ion densities reach bulk values. One can conclude that there are no major artificial effects interfering with the properties of the system. It should be possible and is probably necessary to extend this scheme to more sophisticated methodologies. Standard approaches, such as the Ewald [49] and the Lekner [50] summation techniques and methods based upon these approaches, may be not be immediately appropriate, since these methods do not accommodate mutual polarization effects. On the other hand, the terms in Eqs. (28) and (31) depend on a (screened) $1/r$ term, so it seems likely that aforementioned summation methods could possibly be used in their current form. However, a detailed analysis should be performed to assert the correctness of this statement. The analysis could lead to a new boundary condition model in the framework of the present formulation. In particular, it should be noted that the neutrality of the system in this method may not be fully guaranteed due to polarized charges. Also the treatment of the normal derivative of the fundamental solution in Eqs. ((29),(30)) might not be so straightforward, despite the fact that Eq. (28) just contains an $1/r$ term. The issue of calculating electrostatic forces in a BEM framework was also addressed in detail by Lu et al. [29,30,33]. It should be noted that in a dynamical simulation that relies on dielectric boundaries and explicit ions, such as in this work, if ions enter a low dielectric region the energy may suffer from large fluctuations, which will also affect the forces.

It is expected that the present formulation will be most suitable when employed in coarse-grained simulation models, where the number of degrees of freedom has been considerably reduced to be able to reach longer time scales and simulate at larger length scales than is currently possible with, for instance, molecular dynamics simulation [51]. Typically, boundary models of this type tend to describe the protein at the atomic level and consider the solvent as a continuum without ionic strength, leading to a model with different levels of description for the protein and the solvent (for instance see references [52,53]). A truly consistent coarse-grained simulation model should describe *both* the solute and the solvent at a similar level. For example a protein could be described as a collection of connected larger units, each unit describing for instance a portion of a side chain. These units are collectively moving in an electrolyte solution and are separated from the solvent by an adjustable dielectric boundary to accommodate for mutual polarization effects, as in the present work.

5. Conclusions

A novel boundary element method has been introduced which can be applied to the case of one solute in an electrolyte solution as well as to the case of two solute molecules at a given distance and orientation. The present work introduces, for the first time, explicit ions in a BEM formulation to describe the solvent as an electrolyte, which significantly increases the validity of the method. The resulting equations can be readily specialized to a case of a single solute in a charge-free solvent, which are then identical to those in reference [17]. The feasibility of the present method was demonstrated by computing, among other things, a measure for the potential of mean force between two solutes by means of a Monte Carlo simulation. Finally, the size of the system matrix is the same whether or not ionic strength is included, in contrast to pure continuum approaches. The method can easily be incorporated into existing simulation schemes, is not limited to 1:1 electrolytes, and is suitable for coarse-grained simulation models.

Acknowledgments

The Academy of Finland is greatly acknowledged for funding this work. We also thank Dr. Xueyu Song of the Department of Chemistry of the Iowa State University, Ames, IA 50011, USA, for providing the exact values of the electrostatic interaction energy in Fig. 2. We are also grateful to Mikki Kallio, Reijo Rasinkangas and Esa Luoma for maintaining the Brutus computing facility at the Department of Biochemistry at the University of Oulu. Mikko Salin of the University of Oulu is thanked for stimulating discussions. Finally, we acknowledge Matti McCambridge for proof reading the manuscript.

Appendix A. Matrix-vector formulation

To handle the integral equations (29), (30) numerically, various schemes have been proposed. A very simple approach is followed here. The equations are seen to be of the type

$$C_A f(\mathbf{s}) = \int_{\Sigma_A} K(\mathbf{r},\mathbf{s}) f(\mathbf{r}) \mathrm{d}\sigma + \int_{\Sigma_B} K(\mathbf{r},\mathbf{s}) g(\mathbf{r}) \mathrm{d}\sigma + Q(\mathbf{s}), \tag{33}$$

$$C_B g(\mathbf{t}) = \int_{\Sigma_A} K(\mathbf{r},\mathbf{t}) g(\mathbf{r}) \mathrm{d}\sigma + \int_{\Sigma_B} K(\mathbf{r},\mathbf{t}) f(\mathbf{r}) \mathrm{d}\sigma + Q(\mathbf{t}), \tag{34}$$

where $f(\mathbf{r}) = (\epsilon_S - \epsilon_A)\varphi_A(\mathbf{r})$ and $f(\mathbf{r}) = (\epsilon_S - \epsilon_B)\varphi_B(\mathbf{r})$ with $\mathbf{r} \in \Sigma_A$ and $\mathbf{r} \in \Sigma_B$. The source terms in Eqs. (29) and (30) are represented by the Coulomb potential $Q(\mathbf{s}) = \Sigma_i q_i/\epsilon_0 F(\mathbf{r},\mathbf{s})$, where the sum is over *all* charges. The constants are $C_A = (\epsilon_S + \epsilon_A)/[2(\epsilon_S - \epsilon_A)]$ and $C_B = (\epsilon_S + \epsilon_B)/[2(\epsilon_S - \epsilon_B)]$ and the kernel $K(\mathbf{r},\mathbf{s}) = \frac{\partial F(\mathbf{r},\mathbf{s})}{\partial n}$.

To proceed, the functions f and g are discretized on so-called collocation points, according to

$$f(\mathbf{r}) = \sum_i w_i(\mathbf{r}_i,\mathbf{r}) f_i, \tag{35}$$

$$g(\mathbf{r}) = \sum_j w_j(\mathbf{r}_j,\mathbf{r}) g_j. \tag{36}$$

Here, $\mathbf{r}_i$ and $\mathbf{r}_j$ refer to the collocation points on the boundary of A and B, respectively, and $f_i = f_i(\mathbf{r}_i)$ and $g_j = g_j(\mathbf{r}_j)$ are the values of $f(\mathbf{r})$ and $g(\mathbf{r})$ at $\mathbf{r}_i$ and $\mathbf{r}_j$, respectively. The functions $w(\mathbf{r}_k,\mathbf{r})$ are functions defined only on the boundaries. With Eqs. (35), (36), Eqs. (33), (34) become

$$C_A \sum_k w_k(\mathbf{r}_k,\mathbf{s}) f_k = \sum_i f_i \int_{\Sigma_A} K(\mathbf{r},\mathbf{s}) w_i(\mathbf{r}_i,\mathbf{r}) \mathrm{d}\sigma + \sum_j g_j \int_{\Sigma_B} K(\mathbf{r},\mathbf{s}) w_j(\mathbf{r}_j,\mathbf{r}) \mathrm{d}\sigma + Q(\mathbf{s}) \tag{37}$$

$$C_B \sum_l w_l(\mathbf{r}_l,\mathbf{t}) g_l = \sum_i g_i \int_{\Sigma_A} K(\mathbf{r},\mathbf{t}) w_i(\mathbf{r}_i,\mathbf{r}) \mathrm{d}\sigma + \sum_j f_j \int_{\Sigma_B} K(\mathbf{r},\mathbf{t}) w_j(\mathbf{r}_j,\mathbf{r}) \mathrm{d}\sigma + Q(\mathbf{t}). \tag{38}$$

Multiplying Eq. (37) from the left with $w_m(\mathbf{r}_m,\mathbf{s})$ with $\mathbf{r}_m$, $\mathbf{s} \in \Sigma_A$ and integrating over Σ_A, it is found that

$$\begin{aligned} C_A \sum_k f_k \int_{\Sigma_A} w_k(\mathbf{r}_k,\mathbf{s}) w_m(\mathbf{r}_m,\mathbf{s}) \mathrm{d}\sigma_s = {} & \sum_i f_i \int_{\Sigma_A} \int_{\Sigma_A} K(\mathbf{r},\mathbf{s}) w_i(\mathbf{r}_i,\mathbf{r}) w_m(\mathbf{r}_m,\mathbf{s}) \mathrm{d}\sigma \, \mathrm{d}\sigma_s \\ & + \sum_j g_j \int_{\Sigma_A} \int_{\Sigma_B} K(\mathbf{r},\mathbf{s}) w_j(\mathbf{r}_j,\mathbf{r}) w_m(\mathbf{r}_m,\mathbf{s}) \mathrm{d}\sigma \, \mathrm{d}\sigma_s + \int_{\Sigma_A} Q(\mathbf{s}) w_m(\mathbf{r}_m,\mathbf{s}) \mathrm{d}\sigma_s. \end{aligned} \tag{39}$$

Similarly, multiplying Eq. (38) from the left $w_n(\mathbf{r}_n,\mathbf{t})$ with $\mathbf{r}_n$, $\mathbf{t} \in \Sigma_B$ and integrating over Σ_B, it is found that

$$\begin{aligned} C_B \sum_l g_l \int_{\Sigma_B} w_l(\mathbf{r}_l,\mathbf{t}) w_n(\mathbf{r}_n,\mathbf{t}) \mathrm{d}\sigma_t = {} & \sum_i g_i \int_{\Sigma_B} \int_{\Sigma_A} K(\mathbf{r},\mathbf{t}) w_i(\mathbf{r}_i,\mathbf{r}) w_n(\mathbf{r}_n,\mathbf{t}) \mathrm{d}\sigma \, \mathrm{d}\sigma_t \\ & + \sum_j f_j \int_{\Sigma_B} \int_{\Sigma_B} K(\mathbf{r},\mathbf{t}) w_j(\mathbf{r}_j,\mathbf{r}) w_n(\mathbf{r}_n,\mathbf{t}) \mathrm{d}\sigma\sigma_t + \int_{\Sigma_B} Q(\mathbf{t}) w_n(\mathbf{r}_n,\mathbf{t}) \mathrm{d}\sigma_t. \end{aligned} \tag{40}$$

In a matrix-vector notation, Eqs. (39), (40) are written as

$$C_A \sum_k U_{mk} f_k - \sum_i K_{mi} f_i - \sum_j L_{mj} g_j = P_m, \tag{41}$$

$$C_B \sum_l V_{nl} g_l - \sum_i M_{ni} g_i - \sum_j N_{nj} f_j = Q_n, \tag{42}$$

where

$$U_{ij} = \int_{\Sigma_A} w_j(\mathbf{r}_j,\mathbf{s}) w_i(\mathbf{r}_i,\mathbf{s}) \mathrm{d}\sigma_s, \tag{43}$$

$$V_{ij} = \int_{\Sigma_B} w_j(\mathbf{r}_j, \mathbf{t}) w_i(\mathbf{r}_i, \mathbf{t}) \mathrm{d}\sigma_t, \tag{44}$$

$$K_{ij} = \int_{\Sigma_A} \int_{\Sigma_A} K(\mathbf{r}, \mathbf{s}) w_j(\mathbf{r}_j, \mathbf{r}) w_i(\mathbf{r}_i, \mathbf{s}) \mathrm{d}\sigma \, \mathrm{d}\sigma_s, \tag{45}$$

$$L_{ij} = \int_{\Sigma_A} \int_{\Sigma_B} K(\mathbf{r}, \mathbf{s}) w_j(\mathbf{r}_j, \mathbf{r}) w_i(\mathbf{r}_i, \mathbf{s}) \mathrm{d}\sigma \, \mathrm{d}\sigma_s, \tag{46}$$

$$M_{ij} = \int_{\Sigma_B} \int_{\Sigma_A} K(\mathbf{r}, \mathbf{t}) w_j(\mathbf{r}_j, \mathbf{r}) w_i(\mathbf{r}_i, \mathbf{t}) \mathrm{d}\sigma \, \mathrm{d}\sigma_t, \tag{47}$$

$$N_{ij} = \int_{\Sigma_B} \int_{\Sigma_B} K(\mathbf{r}, \mathbf{t}) w_j(\mathbf{r}_j, \mathbf{r}) w_i(\mathbf{r}_i, \mathbf{t}) \mathrm{d}\sigma \sigma_t, \tag{48}$$

$$P_i = \int_{\Sigma_A} Q(\mathbf{r}) w_i(\mathbf{r}_i, \mathbf{r}) \mathrm{d}\sigma, \tag{49}$$

$$Q_i = \int_{\Sigma_B} Q(\mathbf{r}) w_i(\mathbf{r}_i, \mathbf{r}) \mathrm{d}\sigma. \tag{50}$$

Matrices U and V are termed 'overlap' matrices.

To proceed further, the surface is divided into boundary elements, so that $\int_\Sigma = \sum_k \int_{\Sigma_k}$ becomes a sum of integrals over boundary elements. Also, we let a collocation point $\mathbf{r}_i$ correspond to the center of boundary element Σ_i. Finally, if we let $w_i(\mathbf{r}_i, \mathbf{r})$ be of the form

$$\begin{aligned} w(\mathbf{r}_i, \mathbf{r}) \quad &= \tfrac{1}{\Delta_i} \quad \mathbf{r}_i \in \Sigma_i, \\ &= 0 \quad \mathbf{r}_i \notin \Sigma_i, \end{aligned} \tag{51}$$

where Δ_i is the total area of element i, L_{ij} becomes

$$L_{ij} = \frac{1}{\Delta_i \Delta_j} \int_{\Sigma_i^{(A)}} \mathrm{d}\sigma_s \int_{\Sigma_j^{(B)}} \mathrm{d}\sigma K(\mathbf{r}, \mathbf{s}), \tag{52}$$

where the superscripts (A) in $\Sigma_i^{(A)}$ and (B) in $\Sigma_j^{(B)}$ are to indicate that element i and j belong to the boundary of A and B, respectively.

Eq. (51) corresponds to assuming that the unknowns $f(\mathbf{r})$ and $g(\mathbf{r})$ are constant over each boundary element and are given as the average of the values of f and g over the boundary element. Eq. (52) can easily be computed by numerical means to a desired accuracy [16]. Some care must be taken when i and j both refer to the same boundary element [17] (in K_{ij} and N_{ij}). Eqs. (43), (44) and (46–50) can be treated in a similar fashion as L_{ij}. Also Eqs. (16), (17) and (20) can be computed along similar lines. For instance, P_i becomes

$$P_i = \frac{1}{\Delta_i} \int_{\Sigma_i^{(A)}} \mathrm{d}\sigma Q(\mathbf{r}),$$

where the integration is over boundary element i located on the boundary of A. Note that U_{ij} (and V_{ij}) becomes

$$\begin{aligned} U_{ij} = \quad &\Delta_i^{-1} \quad \text{if } i = j, \\ &0 \quad \text{if } i \neq j. \end{aligned} \tag{53}$$

The matrix Eqs. (41, 42) can be combined into a single matrix equation

$$(\mathbf{c}^{\mathrm{T}}\mathbf{I} - \mathbf{S})\mathbf{x} = \mathbf{b}. \tag{54}$$

If $n = n_A + n_B$ is the total number of collocation points (boundary elements), then the vector $\mathbf{x}$ of length n represents the unknowns $f_i = x_i$ ($i = 1, n_A$) and $g_j = x_{n_A+j}$ ($j = 1, n_B$) and the right-hand-side $\mathbf{b}$ of length n represents the source terms P_i and Q_i in Eqs. ((33), (34)). $\mathbf{I}$ is a diagonal matrix carrying the matrix elements U_{ii} and V_{jj} and $\mathbf{c}$ is a vector for which $c_i = C_A$ for $i = 1, n_A$ and $c_i = C_B$ for $i = n_A + 1, n_A + n_B$. The superscript T refers to the transpose of $\mathbf{c}$. $\mathbf{S}$ contains the kernels K, L, M and N. Eq. (54) can be solved for $\mathbf{a}$ by means of LU decomposition methods [41] or iterative procedures [42]. This work relies on the LU-decomposition method.

After the solution of the matrix Eq. (54) is obtained, it is required to integrate over the boundaries of A and B to obtain the potential due to the boundaries, Eqs. (16), (17) and (20). For instance, with the collocation method presented in this Appendix, the contribution $\varphi_{\mathrm{A}}^{(\mathrm{b})}(\mathbf{r}_k^{\mathrm{A}})$ at $\mathbf{r}_k$ to the total potential $\varphi_{\mathrm{A}}(\mathbf{r}_k^{\mathrm{A}})$ arising from the surface integrals in Eq. (16) becomes

$$\varphi_{\mathrm{A}}^{(\mathrm{b})}(\mathbf{r}_k^{\mathrm{A}}) = \frac{1}{\epsilon_{\mathrm{A}}} \sum_i \frac{f_i}{\Delta_i} \int_{\Sigma_i^{(A)}} K(\mathbf{r}, \mathbf{r}_k) \mathrm{d}\sigma + \frac{1}{\epsilon_{\mathrm{A}}} \sum_j \frac{g_j}{\Delta_j} \int_{\Sigma_k^{(B)}} K(\mathbf{r}, \mathbf{r}_k) \mathrm{d}\sigma \tag{55}$$

or, as a matrix-vector equation,

$$\varphi_{A,k}^{(\mathrm{b})} = \frac{1}{\epsilon_{\mathrm{A}}} \sum_i X_{ki} f_i + \frac{1}{\epsilon_{\mathrm{A}}} \sum_j Y_{kj} g_j \tag{56}$$

with

$$X_{ij} = \frac{1}{\Delta_j} \int_{\Sigma_j^{(A)}} K(\mathbf{r}, \mathbf{r}_i) \mathrm{d}\sigma \tag{57}$$

and

$$Y_{ij} = \frac{1}{\Delta_j} \int_{\Sigma_j^{(B)}} K(\mathbf{r}, \mathbf{r}_i) \mathrm{d}\sigma. \tag{58}$$

These equations can be combined into a single equation of the form

$$\mathbf{\Phi}^{(\mathrm{b})} = \frac{1}{\epsilon_{\mathrm{A}}} \mathbf{Z}\mathbf{x}, \tag{59}$$

where the matrix $\mathbf{Z}$ now contains both $\mathbf{X}$ and $\mathbf{Y}$. Almost identical equations but with a different prefactor ($\epsilon_{\mathrm{A}}^{-1}$) can be derived for the surface integrals of Eqs. (17) and (20).

References

[1] T. Simonson, Electrostatics and dynamics of proteins, Rep. Prog. Phys. 66 (2003) 737–787.
[2] B. Honig, A. Nicholls, A classical electrostatics in biology and chemistry, Science 268 (1995) 1144–1149.
[3] F. Fogolari, A. Brigo, H. Molinari, The Poisson–Boltzmann equation for biomolecular electrostatics: a tool for structural biology, J. Mol. Recognit. 15 (2002) 377–392.
[4] A.H. Elcock, D.Sept.J.A. McCammon, Computer simulation of protein–protein interactions, J. Phys. Chem. B 105 (2001) 1504–1518.
[5] S. Donnini, A.H. Juffer, Calculation of affinities of peptides for proteins, J. Comput. Chem. 25 (2004) 393–411.
[6] D. Bashford, M. Karplus, pK_a's of ionizable groups in proteins: atomic detail from a continuum electrostatic model, Biochemistry 29 (1990) 10219–10225.
[7] A.H. Juffer, P. Argos, H.J. Vogel, Calculating acid dissociation constants using the boundary element method, J. Phys. Chem. B 101 (1997) 7664–7673.
[8] K.A. Sharp, Calculation of HyHel10-lysozyme binding free energy changes: Effect of 10 point mutations, Proteins 33 (1998) 39–48.
[9] A.A. Rashin, Continuum electrostatics and hydration phenomena, Int. J. Quantum Chem.: Quantum Biol. Symp. 15 (1988) 103–118.
[10] Y.N. Vorobjev, J.C. Almagro, J. Hermans, Discrimination between native and intentionally misfolded conformations of proteins: ES/IS, a new method for calculating conformational free energy that uses both dynamics simulations with an explicit solvent and an implicit solvent continuum model, Proteins 32 (1998) 399–413.
[11] A.H. de Vries, P.Th. van Duijnen, A.H. Juffer, J.A.C. Rullmann, J.P. Dijkman, H. Merenga, B.T. Thole, Implementation of reaction field methods in quantum chemistry computer codes, J. Comput. Chem. 16 (1995) 37–55.
[12] D.M. Chipman, Comparison of solvent reaction field representations, Theor. Chem. Acc. 107 (2002) 80–89.
[13] C.J.F. Böttcher, O.C. van Belle, P. Bordewijk, A. Rip, in: Theory of electric polarization, second ed.Dielectrics in Static Fields, I, Elsevier Scientific Publishing Company, Amsterdam, 1973.
[14] J. Warwicker, H.C.J. Watson, Calculation of the electric potential in the active site cleft due to α-helix dipoles, J. Mol. Biol. 157 (1982) 671–679.
[15] I. Klapper, R. Hagstrom, R. Fine, K. Sharp, B. Honig, Focusing of electric fields in the active site of Cu–Zn superoxide dismutase: effects of ionic strength and amino-acid modification, Proteins 1 (1986) 47–59.
[16] R.J. Zauhar, R.S.J. Morgan, A new method for computing the macromolecular electric potential, J. Mol. Biol. 186 (1985) 815–820.
[17] A.H. Juffer, E.F.F. Botta, B.A.M. van Keulen, A. van der Ploeg, H.J.C. Berendsen, The electric potential of a macromolecule in a solvent: a fundamental approach, J. Comput. Phys. 97 (1991) 144–171.

[18] B.J. Yoon, A.M.J. Lenhoff, A boundary element method for molecular electrostatics with electrolyte effects, J. Comput. Chem. 11 (1990) 1080–1086.
[19] A.J. Bordner, G.A. Huber, Boundary element solution of the linear Poisson–Boltzmann equation and a multipole method for the rapid calculation of forces on macromolecules in solution, J. Comput. Chem. 24 (2003) 353–367.
[20] Z. Zhou, P. Payne, M. Vasquez, N. Kuhn, M. Levitt, Finite-difference solution of the Poisson–Boltzmann equation: complete elimination of self-energy, J. Comput. Chem. 17 (1996) 1344–1351.
[21] N. Baker, M. Holst, F. Wang, Adaptive multilevel finite element solution of the Poisson–Boltzmann equation II. Refinement at solvent-accessible surfaces in biomolecular systems, J. Comput. Chem. 21 (2000) 1343–1352.
[22] N.A. Baker, D. Sept, M.J. Holst, J.A. McCammon, The adaptive multilevel finite element solution of the Poisson–Boltzmann equation on massively parallel computers, IBM J. Res. Devel. 45 (2001) 427–438.
[23] C.M. Cortis, R.A. Friesner, An automatic three-dimensional finite element mesh generation system for the Poisson–Boltzmann equation, J. Comput. Chem. 18 (1997) 1570–1590.
[24] M.K. Gilson, B.H.J. Honig, Calculation of electrostatic potentials in an enzyme active site, Nature 330 (1987) 84–86.
[25] M. Totrov, R. Abagyan, Rapid boundary element solvation electrostatics calculations in folding simulations: Successful folding of a 23-residue peptide, Biopolymers 60 (2001) 124–133.
[26] B.J. Yoon, A.M. Lenhoff, Computation of the electrostatic interaction energy between a protein and charged surface, J. Phys. Chem. 96 (1992) 3130–3134.
[27] H.-X. Zhou, Boundary element solution of macromolecular electrostatic. Interaction energy between two proteins, Biophys. J. 65 (1993) 955–963.
[28] X. Song, The extent of anisotropic interactions between protein molecules in electrolyte solutions, Mol. Simult. 29 (2003) 643–647.
[29] B. Lu, D. Zhang, J.A. McCammon, Computation of electrostatic forces between solvated molecules determined by the Poisson–Boltzmann equation using a boundary element method, J. Chem. Phys. 122 (2005) 214102–214108.
[30] B. Lu, X. Cheng, T. Hou, J.A. McCammon, Calculation of the Maxwell stress tensor and the Poisson–Boltzmann force on a solvated molecular surface using hypersingular boundary integrals, J. Chem. Phys. 123 (2005) 84904–84911.
[31] M. Costabel, D.F. Vallejo, J.R. Grigera, Electrostatic recognition between enzyme and inhibitor:, Interaction between Papain and Leupeptin Archives of Biochemistry and Biophysics 394 (2001) 161–166.
[32] W. Chen, B.Z. Lu, C. Wang, A simulation method of combining boundary element method with generalized Langevin dynamics, Chi. Sci. Bull. 45 (2000) 2227–2231.
[33] B.Z. Lu, C.X. Wang, W.Z. Chen, S.Z. Wan, Y.Y. Shi, A stochastic dynamics simulation study associated with hydration force and friction memory effect, J. Phys. Chem. B 104 (2000) 6877–6883.
[34] A.H. Juffer, C.M. Shepherd, H.J. Vogel, Protein-membrane electrostatic interactions: application of the Lekner summation technique, J. Chem. Phys. 114 (2001) 1892–1905.
[35] M. Holst, R.E. Kozack, F. Saied, S. Subramaniam, Treatment of electrostatic effects in proteins: multigrid-based Newton iterative method for solution of the full non-linear Poisson–Boltzmann equation, Proteins 18 (1994) 231–245.
[36] Y.N. Vorobjev, J.A. Grant, H.A. Scheraga, A combined iterative and boundary element approach for the solution of the non-linear Poisson–Boltzmann equation, J. Am. Chem. Soc. 114 (1992) 3189–3196.
[37] A.H. Boschitsch, M.O. Fenley, Hybrid boundary element and finite difference method for solving the non-linear Poisson–Boltzmann equation, J. Comput. Chem. 25 (2004) 935–955.
[38] H.L. Friedman, A Course in Statistical Mechanics, Prentice-Hall Inc, New Jersey, 1985.
[39] J.M.G. Barthel, H. Krienke, W. Kunz, Physical Chemistry of Electrolyte Solutions, Modern Aspects, Springer, New York, 1998.
[40] M. Jardat, O. Bernard, P. Turq, Transport coefficients of electrolyte solutions from smart Brownian dynamics simulations, J. Phys. Chem. 110 (1999) 7993–7999.
[41] W.H. Press, S.A. Teukolsky, W.T. Vettering, B.P. Flannery, Numerical Recipes in C++. The Art of Scientific Computing, second ed., Cambridge University Press, Cambridge, 2002.
[42] F.B. Hildebrand, Introduction to Numerical Analysis, Dover publications, New York, 1987.
[43] M.P. Allen, D.J. Tildesley, Computer Simulation of Liquids, Clarendon Press, Oxford, 1987.
[44] D.J. Evans, On the representation of orientation space, Mol. Phys. 34 (1977) 317–325.
[45] F.J. Vesely, Angular Monte Carlo integration using quaternions parameters: a spherical reference potential for CCl_4, J. Comput. Phys. 47 (1982) 291–296.
[46] C.M. Shepherd, K.A. Schaus, H.J. Vogel, A.H. Juffer, A molecular dynamics study of peptide-bilayer adsorption, Biophys. J. 80 (2001) 579–596.
[47] A.H. Juffer, H.J. Vogel, A flexible triangulation method to describe the solvent-accessible surface of biopolymers, J. Comput.-Aided Mol. Design. 12 (1998) 289–299.
[48] T.E. Creighton, Proteins Structures and Molecular Properties, Freeman, New York, 1992.
[49] P. Ewald, Die Berechnung optischer und elektrostatischer Gitterpotentiale, Ann. Phy. 64 (1921) 253–287.
[50] J. Lekner, Summation of Coulomb fields in computer-simulated disordered systems, Phys. A 176 (1991) 485–498.
[51] H.J.C. Berendsen, Reality simulation – observe while it happens, Science 294 (2001) 2304–2305.
[52] M. Schaefer, M.A. Karplus, A comprehensive analytical treatment of continuum electrostatics, J. Phys. Chem. 100 (1996) 1578–1599.
[53] T. Simonson, Electrostatic free energy calculations for macromolecules: a hybrid molecular dynamics/continuum electrostatics approach, J. Phys. Chem. B 104 (2000) 6509–6513.
[54] G. Melacini, Q. Zhu, M. Goodman, Multiconformational NMR analysis of sandostatin (octreotide): Equilibrium between β-sheet and partially helical structures, Biochemistry 36 (1997) 1233–1241.

[55] E. Lindahl E, B. Hess, D. van der Spoel, Gromacs 3.0: A package for molecular simulation and trajectory analysis, J. Mol. Mod. 7 (2001) 306–317.
[56] W. Humphrey, A. Dalke, .K. Schulten, VMD – visual molecular dynamics, J. Mol. Graphics 14 (1996) 33–38.
[57] S.L. Carnie, D.Y.C. Chan, Interaction energy between identical spherical colloidal particles: the linearized Poisson–Boltzmann theory, J. Colloid Interf. Sci. 155 (1993) 297–312.